

Variability of fCO2 in the Eastern Tropical Atlantic from a moored buoy

Nathalie Lefèvre, Antoine Guillot, Laurence Beaumont, Théo Danguy

▶ **To cite this version:**

Nathalie Lefèvre, Antoine Guillot, Laurence Beaumont, Théo Danguy. Variability of fCO2 in the Eastern Tropical Atlantic from a moored buoy. Journal of Geophysical Research, 2008, 113, pp.C01015. 10.1029/2007JC004146 . hal-00770572

HAL Id: hal-00770572
https://hal.science/hal-00770572

Submitted on 30 Jul 2021

HAL is a multi-disciplinary open access archive for the deposit and dissemination of scientific research documents, whether they are published or not. The documents may come from teaching and research institutions in France or abroad, or from public or private research centers.

L'archive ouverte pluridisciplinaire **HAL**, est destinée au dépôt et à la diffusion de documents scientifiques de niveau recherche, publiés ou non, émanant des établissements d'enseignement et de recherche français ou étrangers, des laboratoires publics ou privés.

Copyright

Variability of fCO_2 in the Eastern Tropical Atlantic from a moored buoy

Nathalie Lefèvre,[1] Antoine Guillot,[2] Laurence Beaumont,[3] and Théo Danguy[3]

Received 6 February 2007; revised 21 September 2007; accepted 9 November 2007; published 23 January 2008.

[1] A fCO_2 sensor, based on a colorimetric method used for the CARIOCA buoys, has been installed on a Pilot Research Moored Array in the Tropical Atlantic (PIRATA) mooring at 6°S, 10°W, in the gulf of Guinea, in June 2006 during the EGEE 3 cruise. Hourly fCO_2 data recorded from June to December 2006 are presented. An alkalinity-salinity relationship has been determined using data from different cruises, which allows the calculation of dissolved inorganic carbon. Although the tropical Atlantic is an important source of CO_2, an unexpected area of low CO_2 concentrations is observed in the South Equatorial Counter Current with fCO_2 values close to equilibrium conditions or even slightly undersaturated with respect to the atmospheric fCO_2 value of 367.7 μatm measured during the cruise. At the end of June, an increase of seawater fCO_2 to 400 μatm is consistent with the beginning of the upwelling season occurring from July to September. Although the mooring is not located within the upwelling area, the spreading of the cold tongue explains the large CO_2 outgassing. The monthly CO_2 flux ranges from 1.19 mmol m^{-2} d^{-1} in June to a maximum of 8.37 mmol m^{-2} d^{-1} in October, when high fCO_2 values above 420 μatm are maintained by the warming of surface water. Most of the fCO_2 distribution can be explained by physical processes and a strong relationship between fCO_2 and SST is determined for the upwelling season. From mid-September, diurnal cycles can be detected. Using a dissolved inorganic carbon budget, periods where net community production or diurnal warming and cooling dominates are observed.

Citation: Lefèvre, N., A. Guillot, L. Beaumont, and T. Danguy (2008), Variability of fCO_2 in the Eastern Tropical Atlantic from a moored buoy, *J. Geophys. Res.*, *113*, C01015, doi:10.1029/2007JC004146.

1. Introduction

[3] The tropical Atlantic is the second most intense oceanic source of CO_2 for the atmosphere after the equatorial Pacific. Although several cruises have sampled the region, the estimate of the CO_2 flux and its spatial and temporal variability are not well determined yet. Each year, in spring-summer an important equatorial upwelling develops in the eastern part of the Atlantic, bringing cold and CO_2-rich waters to the surface. As these waters warm up westward, the fugacity of CO_2 (fCO_2) increases in the ocean leading to an increasing outgassing of CO_2 that is stronger in July than in January [*Andrié et al.*, 1986; *Oudot et al.*, 1995]. The thermocline is shallower in the eastern part of the basin, and seasonal variations of sea surface temperature (SST) are greater in the Gulf of Guinea than in the western tropical Atlantic [*Merle*, 1980]. The Gulf of Guinea is of particular importance as this region is also subject to coastal upwellings. In the northern hemisphere a seasonal coastal upwelling develops between Cape Palmas (Ivory Coast) and Cape three points (Ghana) and Cotonou (Benin) driving the biology of the system [*Hardman-Mountford and McGlade*, 2003] and in the southern hemisphere a coastal upwelling takes place between Gabon and Angola. The major upwelling season occurs between July and September. Along the coasts of Gabon and Angola, the upwelling spreads westward by the advection of the South Equatorial Current (SEC) or the effects of Rossby waves propagation to merge with the equatorial upwelling [*Ajao and Houghton*, 1998] from July to September. Therefore the magnitude of the tropical source of CO_2 will likely depend on the strength of the upwellings. Rivers, such as the Congo, might also affect the surface CO_2 concentration.

[4] In addition to the seasonal variability, the tropical Atlantic exhibits an interannual variability evidenced by warm events sometimes referred to as Atlantic El Niño [*Hisard*, 1980]. They are indeed similar to the Pacific El Niño as they are characterized by a weakening of the trade winds, and hence a decrease of the equatorial upwelling.

[5] The equatorial circulation is very dynamic and short term variations are missed by the coarse time and space scale of research cruises. To document and understand the CO_2 distribution in the tropical Atlantic, it is necessary to monitor the CO_2 variability in the upper ocean. In this context, a CO_2 observational network is being set up as part of the European project CARBOOCEAN. Time-series stations provide a useful means to document the dynamics of the ocean circulation and the seasonal evolution of the

[1] IRD LOCEAN, Université Pierre et Marie Curie, Paris, France.
[2] DT INSU, Bâtiment Institut Polaire, Plouzané, France.
[3] DT INSU, Meudon, France.

Copyright 2008 by the American Geophysical Union.
0148-0227/08/2007JC004146

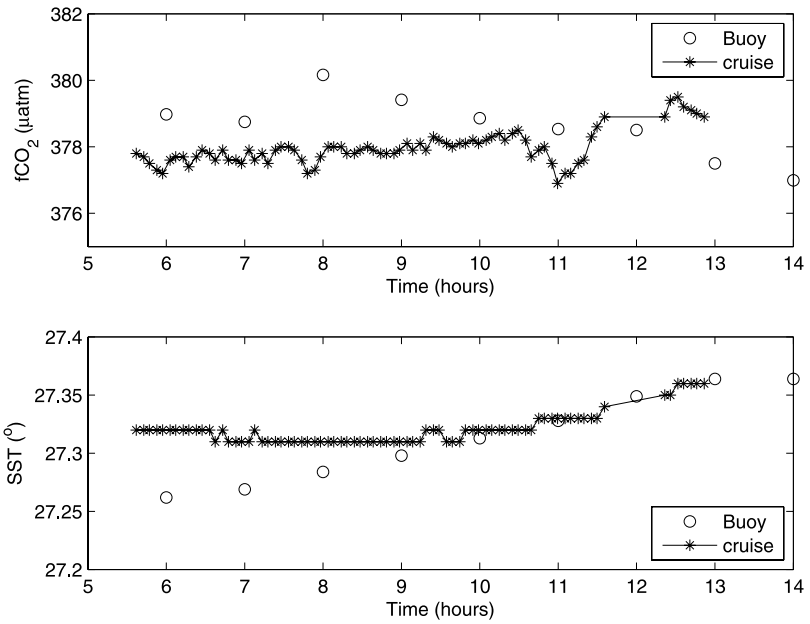


Figure 1. Comparison of SST and fCO_2 between the CO_2 sensor (colorimetric method) and the underway system (infrared detection) on the 7th of June 2006.

fugacity of CO_2. Thus the Hawaiian Ocean Time-series, HOT [*Winn et al.*, 1998], the Bermuda Atlantic Time-series, BATS [*Bates*, 2001] and the European Station for Time series in the Ocean at the Canary islands, ESTOC [e.g., *González Dávila et al.*, 2003] provide long-term records of CO_2. However, these stations require significant ship time to provide monthly monitoring of the CO_2 properties. The technological development of small autonomous in situ CO_2 sensors has led to a new generation of time-series. For example, in the tropical Pacific, some Tropical Atmosphere Ocean (TAO) moorings are now equipped with infrared CO_2 instruments [*Chavez et al.*, 1999] and in the Baltic Sea a SAMI-CO_2 sensor [*DeGrandpre et al.*, 1995] was installed on a moored platform [*Kuss et al.*, 2006] but high frequency measurements are still scarce. In the tropical Atlantic, a program called PIRATA (Pilot Research Moored Array in the Tropical Atlantic) has been set up with the main purpose of studying the ocean-atmosphere interactions that are relevant to regional climate variability on a seasonal, interannual and longer timescales [*Servain et al.*, 1998]. It consists of 15 buoys moored from 38°W to 8°E and 19°S to 15°N that record sea temperature, salinity, at the surface and at several depths. The wind, the precipitations and the atmospheric pressure are also monitored. Adding CO_2 sensors on these moorings provide a good opportunity to record CO_2 as well as some parameters to help interpreting the data. A CO_2 sensor based on the CARIOCA technology [*Bates et al.*, 2000; *Hood and Merlivat*, 2001] has been installed on one of these moorings at 6°S, 10°W in the Gulf of Guinea. This new time-series station setup in the tropical Atlantic will provide high resolution time variability data over multi-months periods. For the first time it will allow us to document the diurnal to seasonal variability of fCO_2 in an undersampled region. On a longer timescale it will give insights into the behavior of the ocean under increasing atmospheric CO_2. The purpose of this paper is to present these new CO_2 data and to analyse the temporal variation of fCO_2 since the beginning of the monitoring in June 2006 until the end of 2006.

2. Methods

[6] The CO_2 sensor measures fCO_2 by the colorimetric method used on the CARIOCA drifting [*Bakker et al.*, 2001; *Hood et al.*, 1999, 2001] or moored buoys [*Bates et al.*, 2000; *Copin-Montegut et al.*, 2004] with an accuracy of ±3 μatm [e.g., *Copin-Montegut et al.*, 2004; *Hood and Merlivat*, 2001]. The sensor is calibrated against fCO_2 measurements made by an infrared detector. In order to setup the time-series in the tropical Atlantic, the CO_2 sensor had to be adapted to be installed on the PIRATA buoy itself. The sensor is located below the buoy at 1.5 m depth and the electronics is located on the platform about 1 m above sea level. A copper pipe has been used to supply seawater to the sensor in order to prevent biofouling. Copper reacts electrochemically with seawater and the oxidation reaction leads to a change of pH, hence a change of fCO_2. However, the sensor is rinsed with 1 liter during 30 s so the exposure time of seawater with copper is very short and does not affect the fCO_2 measurements. The data are sent via Argos separately from the physical parameters of the PIRATA buoy. SEA-BIRD sensors record temperature at the surface, 20 m, 40 m, 60 m, 80 m, 120 m, 300 m, and 500 m. Salinity is measured at the surface, 20 m, 40 m, and 120 m. The buoy is also equipped with a rain gauge and an anemometer. Temperature, salinity, precipitations, wind speed are averaged daily and available on the PIRATA website (http://www.pmel.noaa.gov/pirata).

[7] Hourly fCO_2 and SST measurements are sent in real time. Data are also stored on the buoy to avoid any loss of data in case of transmission problems. The PIRATA buoys are usually serviced once a year so the sensor is designed to

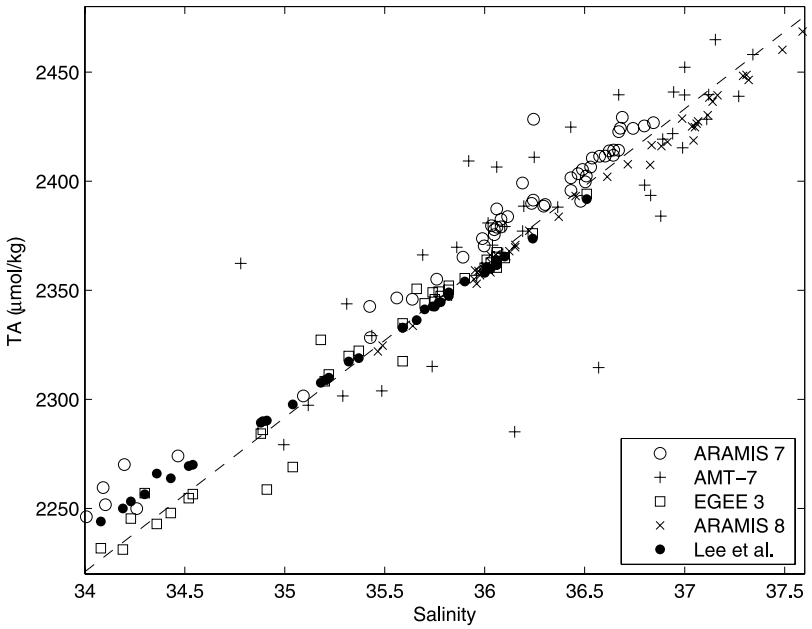


Figure 2. Alkalinity-salinity relationship (dashed line) determined from ARAMIS 7 and AMT-7 data and validated using ARAMIS 8 and EGEE 3 data between 20°S and 20°N. The *Lee et al.* [2006] relationship is shown with black circles.

work unattended for that length of time. The CO_2 sensor will be replaced each year in order to provide a continuous time series.

[8] As the CO_2 sensor has been installed during the EGEE 3 cruise, fCO_2 was also measured using an underway fCO_2 system consisting of a gas-seawater equilibrator and an infrared CO_2 gas analyzer, Licor 7000, which allows a comparison between the two systems. The precision of fCO_2 measurements is estimated to be ±1 μatm. After the buoy was moored at its location, the CO_2 sensor started to transmit its data. Several hours of measurements were made at this location before the ship moved further south along 10°W. The two systems give similar values of fCO_2 and SST (Figure 1).

[9] Alkalinity has been measured during ARAMIS cruises from France to Brazil. Alkalinity was also calculated during the AMT-7 cruise (UK-Uruguay) using DIC and fCO_2 measurements. Using these data between 20°S and 20°N, the following relationship between alkalinity and salinity (S in psu) is established, valid for the salinity range 34–37.5:

$$TA = 70.73(\pm 2.04)S - 183.82(\pm 73.5)\ r^2 = 0.96 \qquad (1)$$

[10] The standard error on the predicted alkalinity is ±11 μmol/kg. This relationship is robust and data from the ARAMIS 8 cruise (April 2006) validate the fit as well as the EGEE 3 data (Figure 2). The TA-S relationship is quite close to the relationship of *Rios et al.* [2005] who obtained a slope of 63 μmol kg^{-1}/psu for the Azores area, and to the *Lee et al.* [2006] relationship. However, it is not valid for Congo waters as a salinity of zero would lead to a negative alkalinity. The salinity measured by the PIRATA buoy is available at daily resolution and is interpolated on an hourly basis, at the CO_2 data resolution. The salinity ranges from 35.6 to 36.3, which suggests that Congo waters do not reach this location. During the EGEE 3 cruise, the surface waters at this location were depleted in nutrients showing that nutrients brought by upwelled and Congo waters were consumed rapidly. From fCO_2 and salinity measurements, dissolved inorganic carbon (DIC) is calculated using the dissociation constants of *Mehrbach et al.* [1973] refitted by *Dickson and Millero* [1987]. An error of 1 μmol/kg in alkalinity leads to an error of 0.8 μmol/kg in DIC when DIC is calculated from fCO_2 and TA. As the error on the predicted alkalinity from salinity is 11 μmol/kg, the resulting error on DIC is 8.8 μmol/kg.

[11] The CO_2 flux (expressed in mmol m^{-2} d^{-1}) is calculated using:

$$F_{CO2} = k_{CO2}\alpha(fCO_{2\,sea} - fCO_{2\,atm}) \qquad (2)$$

where α is the solubility of CO_2 [*Weiss*, 1974], $fCO_{2\,atm}$ is the atmospheric fCO_2 measured during the EGEE 3 cruise (26 May–5 July 2006) and is equal to 367.7 ± 1.8 μatm. The gas exchange piston velocity for CO_2, k_{CO2}, for short-term winds, given by *Wanninkhof* [1992], is used. The daily wind speed available at the mooring, and measured at 4 m, is converted to a 10m wind speed and interpolated at hourly scale.

3. Oceanographic Conditions Near and at the Mooring

[12] The surface layer of the tropical Atlantic is occupied by the warm Tropical Surface Water (TSW), and underneath lies the South Atlantic Central Water [*Stramma and Schott*, 1999]. The mean circulation in the Gulf of Guinea is characterized by upwelling that brings cold and nutrient-and-carbon-rich water to the surface along the equator. This

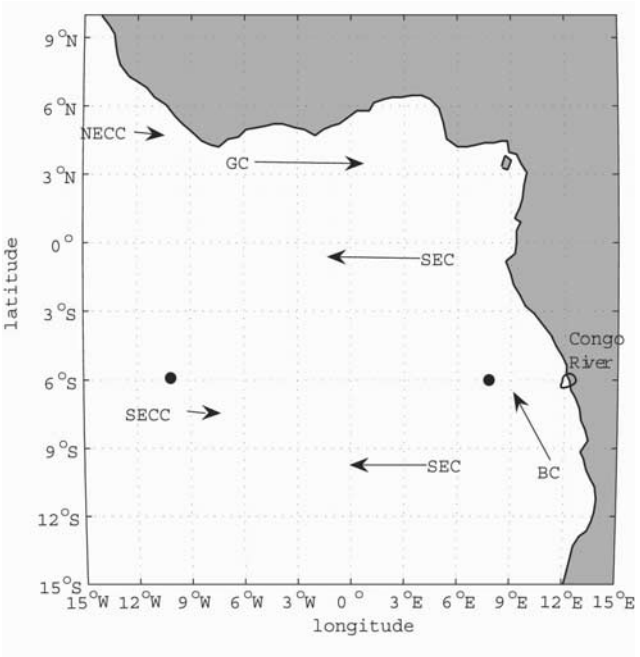


Figure 3. Surface circulation in the Gulf of Guinea showing the North Equatorial Counter Current (NECC), the South Equatorial Current (SEC) and the South Equatorial Counter Current (SECC). The Guinea current (GC) is an extension of the NECC current. The Benguela current (BC) is a coastal equatorward current. The locations of the PIRATA moorings at 6°S, 10°W and at 6°S, 8°E are also indicated (black circles). Only the mooring at 6°S, 10°W is equipped with a CO_2 sensor.

equatorial divergence occurs between about 0 to 4°S. The primary source of this upwelled water, salty and rich in O_2, is the equatorial undercurrent (EUC), which flows eastward across the basin [*Gouriou and Reverdin*, 1992]. The main surface current is the South Equatorial Current (SEC) that flows westward and extends from the surface to 100m. It is found between 4°N to 15–25°S depending on longitudinal location and the time of the year. Upwelled waters are transported by this current and their CO_2 concentration increases as the surface water warms up toward the west [*Andrié et al.*, 1986]. *Molinari* [1982] also observed an eastward current, the South Equatorial Countercurrent (SECC), flowing between 7°S and 9°S (Figure 3). It is formed near 30°W and is a recirculation of the southern branch of the SEC [*Molinari*, 1982]. It is characterized by warm and salty subtropical waters. This current is not very often mentioned as it is difficult to detect in maps of average surface velocity because it is subject to strong seasonal variations in flow directions. However, it was observed during the EGEE 3 cruise (B. Bourlès, personal communication).

[13] In addition to these large-scale currents, the Gulf of Guinea is affected by river discharge with the Congo (at 6°S), second world largest river, which supplies 40,600 m^3/s of freshwater on annual average [*Seyler et al.*, 2003]. The highest flow occurs in December and in May but the extent of the Congo plume and its impact on the biogeochemical properties of the area are still largely unknown. However, low salinities seem to be restricted to a narrow coastal band [*Piton and Kartavtseff*, 1986] suggesting little offshore advection of the Congo River outflow. Since the 29th of June 2006, a new PIRATA buoy is moored at 6°S, 8°E (Figure 3) and should provide more insights on the Congo River outflow. From the beginning of the time series to the 4th of November 2006, the surface salinity has always been higher than 35 and from the 23rd of November the salinity was between 32.5 and 34.5 (PIRATA website). The surface salinity sensor did not provide any data since the 11th of December.

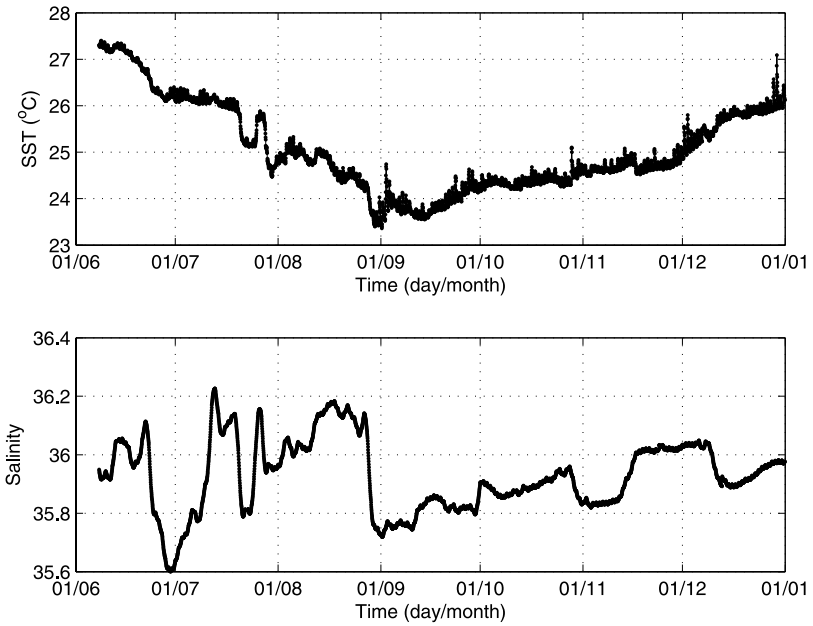


Figure 4. Distribution of temperature and salinity at 6°S, 10°W from 8th of June 2006 to 31 December 2006.

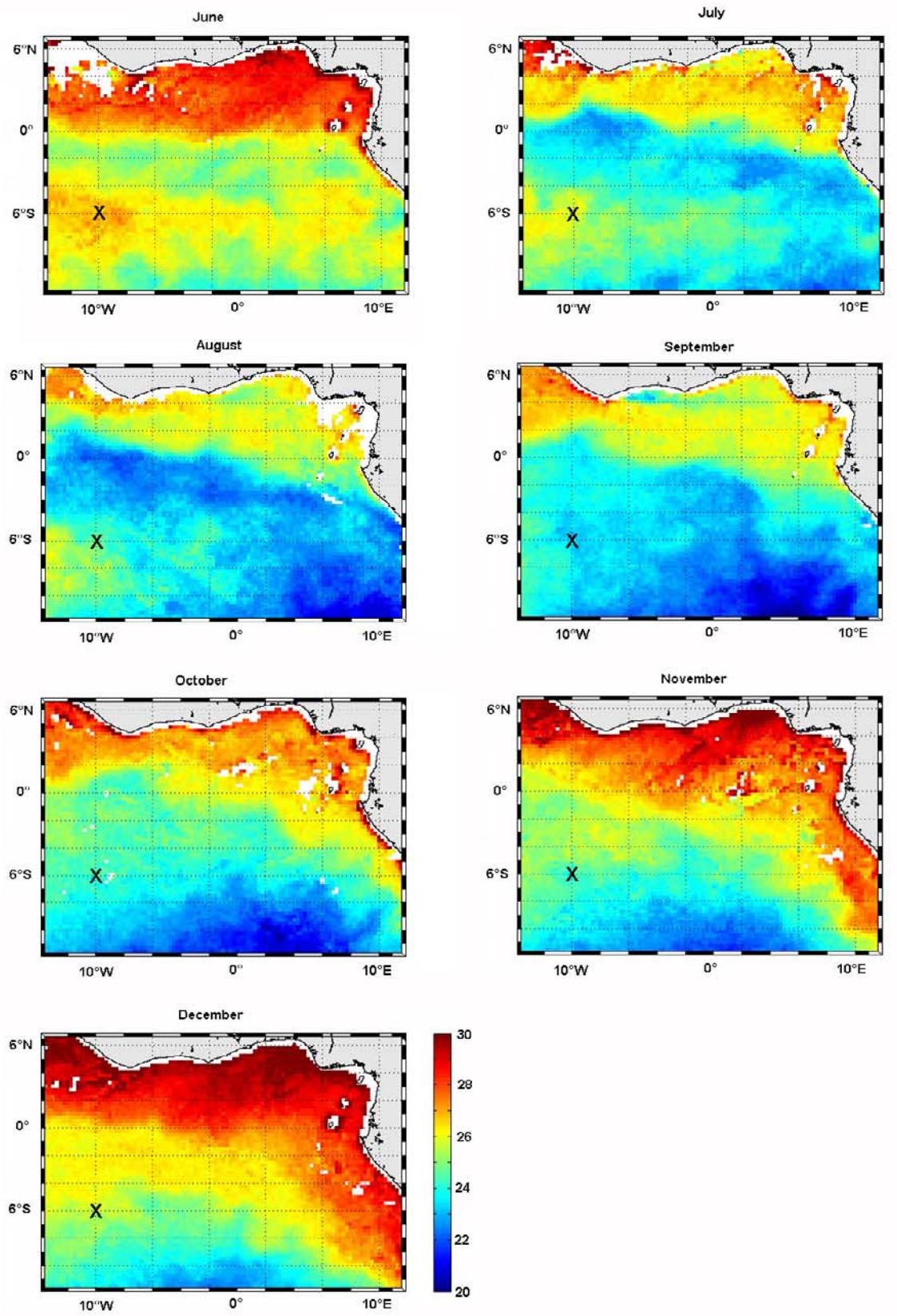


Figure 5. SST TMI imagery (9km resolution) of the Gulf of Guinea. The images are 3 days composites of 15 June, 15 July, 15 August, 15 September, 15 October, 15 November and 15 December 2006. The black cross corresponds to the location of the mooring.

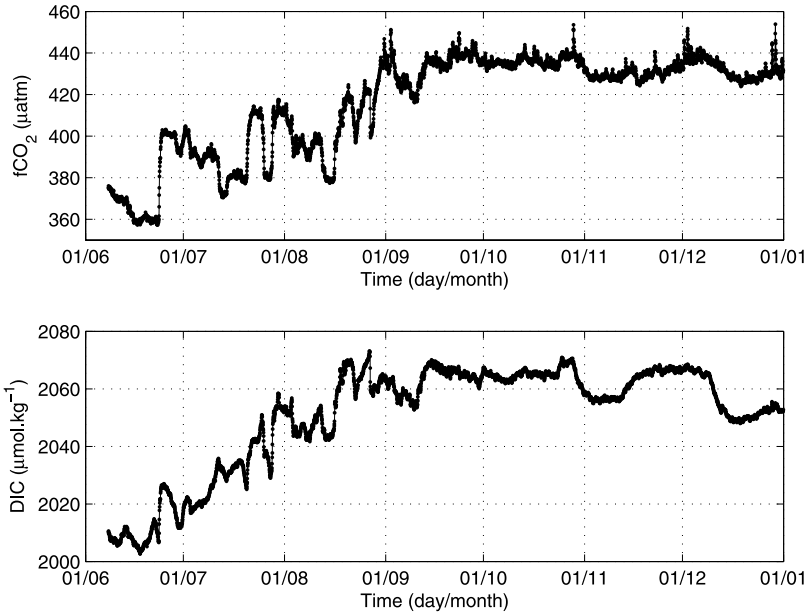


Figure 6. Distribution of fCO_2 and DIC at 6°S, 10°W from 8th June 2006 to the end of December 2006.

[14] At 6°S, 10°W, the buoy is located at the boundary between the westward SEC and the eastward SECC. During the main upwelling season (July to September) the wind comes from the Southeast. The lowest SST, around 23.5°C, is usually observed in August while the maximum SST, around 28.5°C, is reached in April so that the amplitude of the seasonal cycle is about 5°C at this site. From density data σ_ϑ available from the PIRATA mooring the depth of the mixed layer can be calculated using a difference in σ_ϑ of 0.125 kg m^{-3} as a criterion. From June to September the mixed layer is constant at 40m suggesting that the mooring is not subject to local upwelling. However, it is affected by the advection of upwelled waters. The SST decreases throughout the upwelling season and the surface salinity can decrease to 35.6 (Figure 4). At this location, water with the salinity of 35.6 and temperature of 15°C is found at a depth of 120 m. Therefore as the surface temperature remains well above this value, this suggests that the water upwelled closer to the coast and was advected westward. This is confirmed by the satellite imagery of SST on which the spreading of the cold tongue can be seen with cold waters gradually invading the Gulf of Guinea from the south and joining the equatorial upwelling near 10°W, south of the equator, in July (Figure 5). The coldest SST are observed in August and September and from October, surface waters start warming up.

4. Impact of the Upwelling on CO_2 Variations at 6°S, 10°W

[15] fCO_2 variations have been recorded since the 8th of June 2006. DIC is calculated using fCO_2 and the TA-S relationship. The fCO_2 and DIC distributions exhibit low values until the end of June followed by an increase until September and quite stable values afterward (Figure 6). At the beginning of the time-series, the sea surface temperature is high with a value above 27°C and the water is close to equilibrium conditions with respect to atmospheric CO_2 as it is before the onset of the upwelling. This is consistent with the measurements made during the cruise where surface waters are slightly undersaturated with respect to atmospheric CO_2 on the 10°W section south of 5°S. The influence of the eastward SECC, warm and salty, flowing between 6°S and 9°S may explain the CO_2 undersaturations. Before the north-westward spreading of the cold tongue, two main water masses are present: warm and salty waters close to CO_2 equilibrium with the atmosphere, and colder and fresher waters rich in CO_2. This is clearly seen during the EGEE 3 cruise when the ship moves from 10°S, 10°W to 5°S, 5°W. A sharp front occurs near 6.5°S showing the transition between tropical surface water (TSW) and upwelled water (Figure 7).

[16] The TSW is gradually replaced by the progression of the cold tongue and fCO_2 increases with values above 400 μatm, which is consistent with tropical upwelling values. For example, *Bakker et al.* [2001] reported similar values, in the equatorial upwelling, from their drifting buoy in 1997.

[17] Superimposed on the large scale feature of increasing fCO_2 associated with the spreading of upwelled waters, small SST and fCO_2 variations are recorded. Instead of having abrupt temperature and fCO_2 changes as those observed during the cruise, the fCO_2 and SST records are characterized by gradual variations. The SST decreases slowly from June to September and increases of 3°C over 4 months after September. (V-shape of the SST time-series, Figure 4). Within the decreasing trend of SST, peaks and troughs are observed. This pattern can be explained by the location of the mooring not being directly affected by coastal or equatorial upwellings. The spreading of the cold tongue mixes with TSW and generates meanders. Intrusions of tropical warm and salty water are associated with lower fCO_2 values and can be detected more easily once the

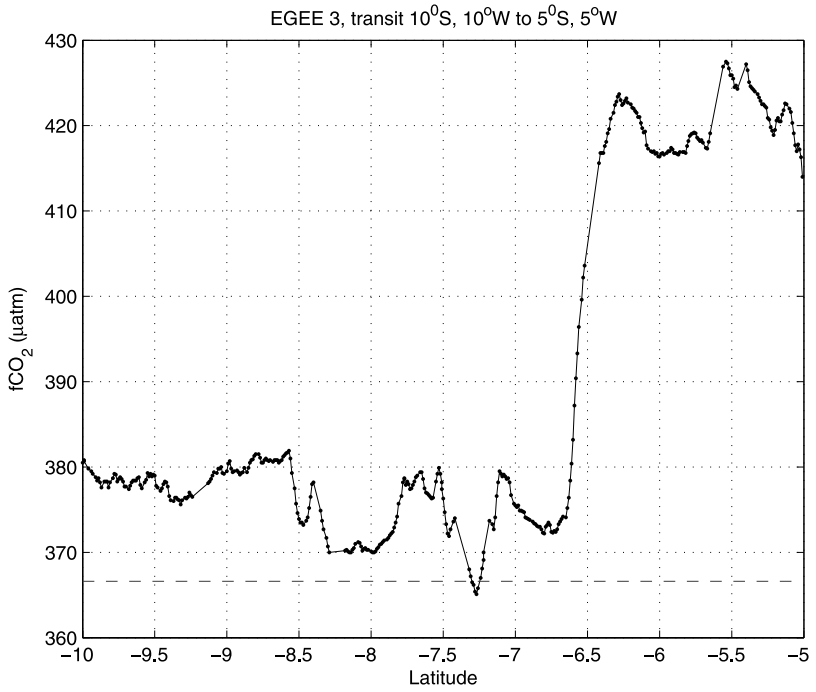


Figure 7. fCO_2 as a function of latitude from 10°S, 10°W to 5°S, 5°W during the EGEE 3 cruise. The dash line corresponds to the mean atmospheric value measured during the cruise.

signals are detrended, i.e., the linear trend is removed from the data, and normalized by dividing the detrended data by their standard deviation (Figure 8).

[18] From June to September the CO_2 variability is mainly driven by the development of the upwelling and strong correlations are observed between temperature, salinity and fCO_2. Temperature and salinity are well correlated

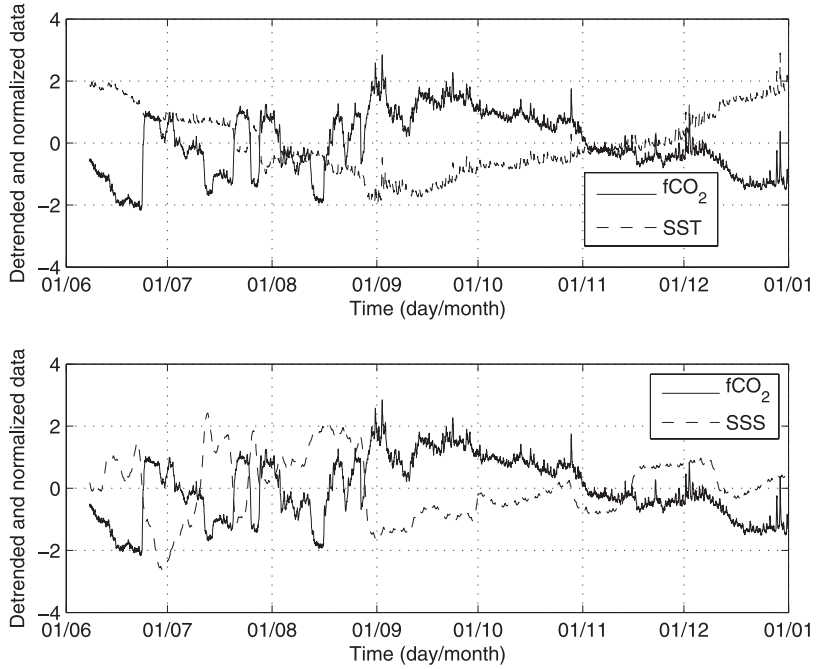


Figure 8. Detrended and normalized fCO_2 and SST as a function of time in day/month (top panel), detrended and normalized fCO_2 and SSS as a function of time (bottom panel). The detrended data are obtained by removing the linear trend. The detrended data are then divided by their standard deviation to normalize them.

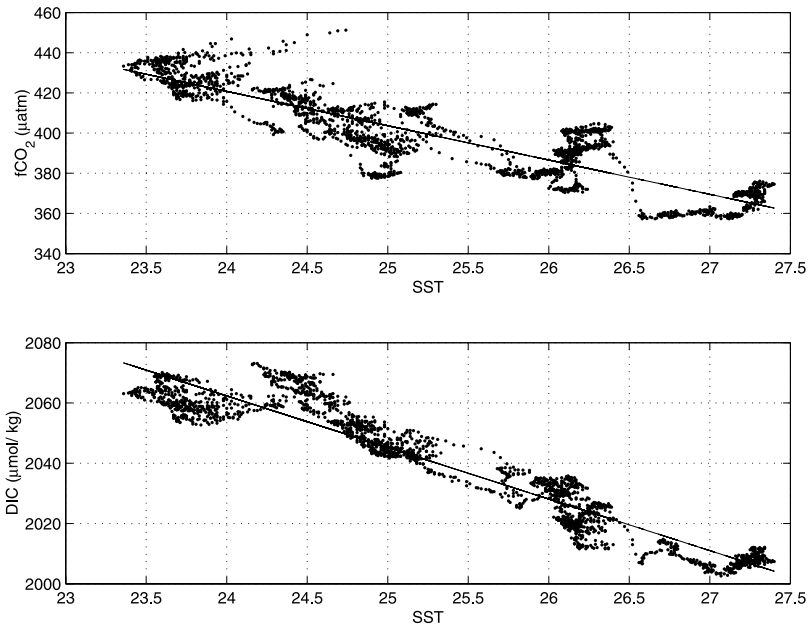


Figure 9. Relationships between fCO_2 and SST (top panel) and DIC and SST (bottom panel) between the 8th of June and the 15th of September 2006.

with warm and saltier waters corresponding to low CO_2 values, and with cold and fresher waters corresponding to upwelled waters rich in CO_2. A relationship between fCO_2 and SST can be determined for the period 8 June to 15 September:

$$fCO_2 = -17.08*SST + 830.7 \qquad \rho = -0.88 \qquad (3)$$

A stronger relationship (correlation coefficient $\rho = -0.95$) is found between DIC and SST:

$$DIC = -17.1\ SST + 2473.1 \qquad (4)$$

for the same period (Figure 9). The upwelling as well as convective mixing supply CO_2 rich waters to the surface so

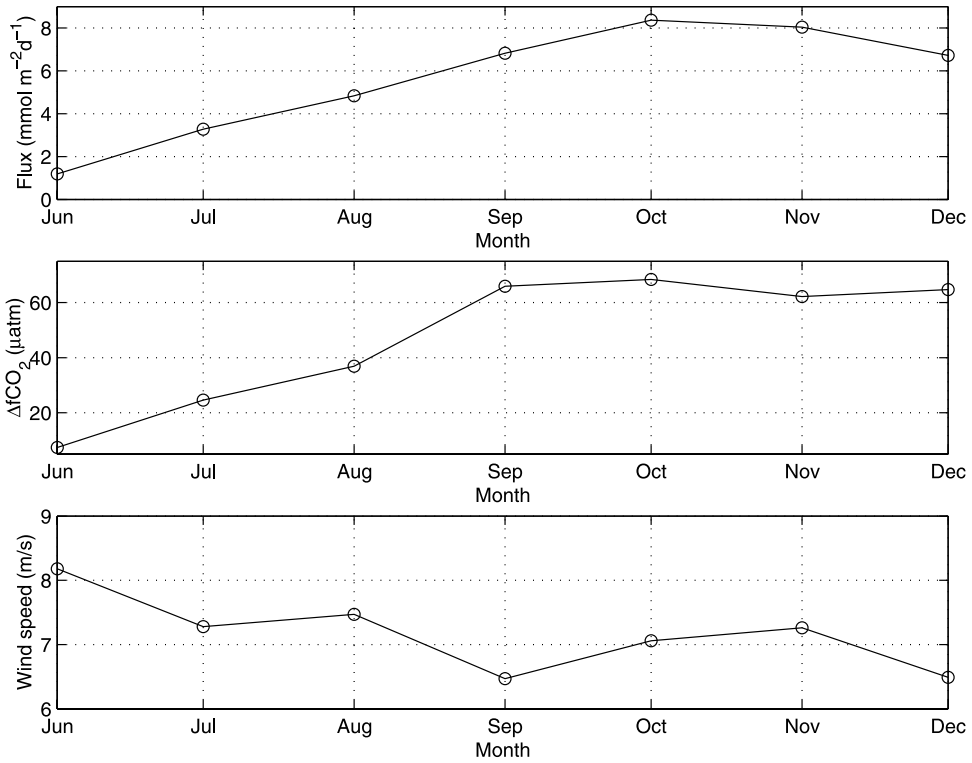


Figure 10. Monthly means of the CO_2 flux (top panel), ΔfCO_2 the difference of fugacity of CO_2 between the ocean and the atmosphere (middle panel) and the wind speed (bottom panel).

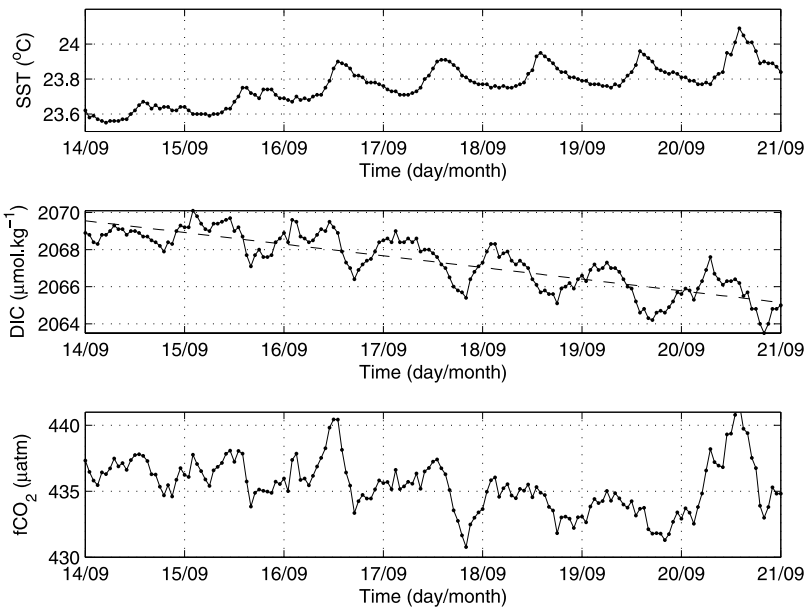


Figure 11. Diurnal cycles of SST, DIC and fCO_2 near the end of the upwelling season (14–20 September).

cold waters are associated with high CO_2 concentrations. The warming of surface waters increases the fugacity of CO_2 and results in high fCO_2 also associated with rather cold temperature around 24.5°C (Figure 9) so the fCO_2-SST relationship is weaker than the DIC-SST one.

[19] After the upwelling season, i.e., from mid-September to December, no correlation between fCO_2 or DIC and SST can be determined. The temperature increases gradually from mid-September and is associated with a constant or slight decrease of fCO_2 (Figures 4 and 6). *Smethie et al.* [1985] and *Oudot et al.* [1987] noticed that warming during horizontal advection of surface water was also an important mechanism to explain high fCO_2 values. As the exchange with the atmosphere is a slow process there is no significant reduction of fCO_2 after the upwelling season. However, the lack of correlation with SST suggests that the solubility effect is not the only process responsible for the CO_2 variations. It might counterbalance the loss of CO_2 to the atmosphere and any biological uptake.

[20] *Oudot et al.* [1995] reported an annual CO_2 flux stronger during the upwelling season (July) than the warm season (January) from the FOCAL cruises. At 6°S, 10°W, the monthly CO_2 flux gradually increases from June (1.19 mmol m^{-2} d^{-1}) to September (6 mmol m^{-2} d^{-1}). A slight increase of wind speed leads to the maximum CO_2 flux in October (Figure 10). Nevertheless, the winds are quite steady, with an average at 7.3 m/s, and most of changes in the outgassing flux is attributed to changes in surface water fCO_2. The warming of the surface waters helps to maintain high surface fCO_2 values so there is no significant reduction of the CO_2 flux from October to December.

5. Diurnal Variability

[21] The spreading of the cold tongue explains the high fCO_2 associated with cold temperatures. The changes from non-upwelling to upwelling conditions are monotonic and the mixing between warm and cold waters account for the peaks and troughs noticed in the time-series. Superimposed on these variations, a diurnal cycle appears.

[22] During the development of the upwelling in June-July, the diurnal cycle is difficult to detect as two main water masses, the TSW and the cold tongue, are present. At the end of the upwelling, season, the diurnal cycle is detected for some short lengths of time, probably because of a relative homogeneity and stability of the surface waters. For example, from the 14th to 21st of September, SST increases from about 23.6°C to 24.1°C with amplitude of the diurnal cycle ranging from less than 0.1°C to 0.3°C. The diurnal variability of DIC ranges from less than 1 to about 3 μmol/kg and decreases of about 5 μmol/kg over the 7 day period (Figure 11). It is more difficult to detect the diurnal variability of fCO_2 because fCO_2 is subject to gas exchange and temperature variations so the correlation coefficient is only -0.13 compared to -0.78 for DIC and SST. For that reason fCO_2 at a given temperature is often used as a proxy for DIC.

[23] Fitting a linear regression to the DIC series leads to a slope of -0.63 μmol kg^{-1} d^{-1}. During the period considered (14–21 September) the mixed layer depth is constant at about 40 m so the total decrease of DIC over this period is $\Delta DIC = -25.2$ mmol m^{-2} d^{-1}. The DIC variations are the result of changes due to loss of carbon to the atmosphere, ΔDIC^a, vertical diffusion between the surface layer and upper layer of the thermocline, ΔDIC^d, the net community production, ΔDIC^b, and precipitation or dissolution of carbonate minerals, ΔDIC^c:

$$\Delta DIC = \Delta DIC^a + \Delta DIC^d + \Delta DIC^b + \Delta DIC^c \qquad (5)$$

[24] The loss of CO_2 to the atmosphere is calculated by the CO_2 flux across the air-sea interface. Over this period,

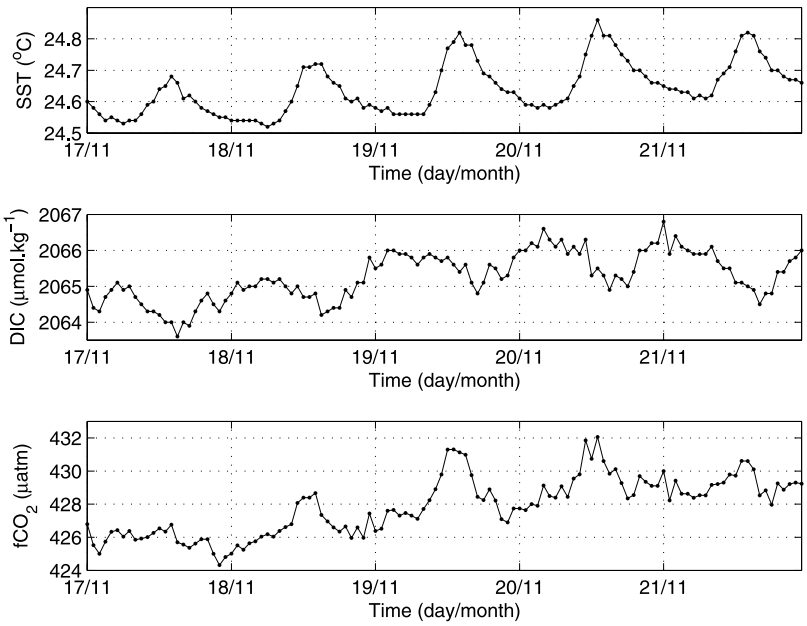


Figure 12. Diurnal cycles of SST, DIC and fCO_2 after the upwelling season (17–21 November).

the mean CO_2 flux is 8.49 mmol m^{-2} d^{-1}. The vertical diffusive flux is expressed by the Fick's law:

$$\Delta DIC^d = K_z \, dC/dz \tag{6}$$

where K_z is the vertical eddy diffusivity for the upper part of the thermocline, C the DIC concentration and z the depth. K_z is very low in tropical areas with strong stratification so we assume that this flux is negligible. *Denman and Gargett* [1983] gave an estimate of K_z of 4.1 m^2 s^{-1}. The change of DIC due to precipitation or dissolution of carbonate minerals is expressed as a function of changes in alkalinity and DIC^b [*Johnson et al.*, 1979] using the average stoichiometric composition of biogenic material P/N/C of 1/16/123 given by *Körtzinger et al.* [2001]:

$$\Delta DIC^c = 0.5\left(\Delta TA + 17/123 \; \Delta DIC^b\right) \tag{7}$$

[25] The net community production is obtained by difference between ΔDIC and the other terms using equation (5) and is found equal to -17.8 mmol m^{-2} d^{-1} (i.e., 211 mgC m^{-2} d^{-1}), which is is a minimum estimate as we neglect the input of carbon from the subsurface layer. However, this estimate is consistent with previous estimates of primary production $\sim$200 mgC m^{-2} d^{-1} reported for typical tropical structures [*Pérez et al.*, 2005], so our assumption is reasonable. At 6°S, 10°W, the mixed layer is nitrate depleted, which characterizes a typical tropical structure [*Herbland and Voituriez*, 1979]. The biological activity is the dominant process responsible for the diurnal changes of DIC over the period 14–21 September. The CO_2 flux is quite significant as it is 48% of the biological DIC variation compared to the 9.5% reported by *Oudot* [1989] for the Guinea Dome area. This can be explained by the larger supersaturation observed at the mooring.

[26] Another period when the diurnal cycle is observed corresponds to a 5-day period in November. The fCO_2 cycle is more in phase with the SST (Figure 12) and the correlation between fCO_2 and SST is very strong (ρ = 0.80) compared to -0.13 for the previous series 14–21 September. Also, the DIC amplitude over the period is much smaller and increases by 0.29 μmol kg^{-1} d^{-1} showing no net carbon uptake over that period. fCO_2 expressed as a function of SST over that period gives:

$$fCO_2 = 17.00 \; SST + 8.85 \tag{8}$$

[27] This corresponds to an increase of 4%/°C which means that the dominant process is the warming of the water mass. This process counterbalances the biological uptake on a daily basis on the fCO_2 signal: fCO_2 maxima are in phase with the SST maxima whereas DIC maxima correspond to SST minima. For this period, the diurnal variability in fCO_2 was primarily controlled by diurnal warming and cooling rather than net community production or gas exchange. This mechanism was also responsible for the fCO_2 diurnal variability observed in the Sargasso Sea [*Bates et al.*, 1998] and in the equatorial Pacific Ocean [*Goyet and Peltzer*, 1997].

6. Conclusions

[28] A new CO_2 time series station has been setup in the tropical Atlantic at 6°S, 10°W to provide high frequency data over multi months period. Hourly fCO_2 and SST data are transmitted by ARGOS. In addition to fCO_2 measurements, data from several cruises are used to determine an alkalinity- salinity relationship for the tropical Atlantic. The calculated alkalinity and the fCO_2 observations are then used to compute dissolved inorganic carbon. This relationship is quite robust so that, knowing salinity and fCO_2, all the parameters of the carbon system can be determined.

[29] The main large scale features of the time series are characterized by a decrease of SST associated with an increase of fCO_2 corresponding to the upwelling that develops from the end of June to September. At the end of the upwelling season, SST increases and fCO_2 remains very high. The CO_2 flux gradually increases from June to reach a maximum of 8.37 mmol m^{-2} d^{-1} in October. Although the upwelling ends in September, the warming of the surface water maintains high fCO_2 values and explains that the strongest outgassing occurs in October. The upwelling signal observed at the mooring is not the result of vertical advection, as the mixed layer remains constant, but of the spreading of a cold tongue caused by the coastal upwelling.

[30] Diurnal variations are observed once the cold tongue has stopped its propagation. A simple DIC budget in the mixed layer shows that they can be explained by biological carbon fixation and solar heating. A net community production of 211 mg C m^{-2} is estimated from this budget.

[31] Monitoring fCO_2 at this location will help in better understanding the temporal variability of fCO_2 and the key controlling processes governing the fCO_2 variability. On a longer timescale, the time series should provide some insights on the impacts of warm and cold years on the fCO_2 distribution.

[32] **Acknowledgments.** We thank Bernard Bourlès, of Institut de Recherche pour le Développement (IRD) Brest, for our participation in his EGEE/AMMA project and the crew members of the R/V *Atalante* for their help during the cruise. We are grateful to Nicolas Martin for sharing his programs to process the CO_2 ARGOS data. Data management for PIRATA moorings is conducted by the TAO project office at NOAA/PMEL in collaboration with many research institutes listed on the PIRATA website (http://www.pmel.noaa.gov/pirata). TMI data are produced by Remote Sensing Systems and sponsored by the NASA Earth Science and REASoN DISCOVER project. They are available at www.remss.com. We are grateful to Dominique Dagorne for retrieving satellite imagery. This work is funded by the European Integrated Project CARBOOCEAN (contract 511176-2), by the IRD, and the Centre National d'Etudes Spatiales (ARAMIS project). The manuscript benefited from the comments of two anonymous reviewers.

References

Ajao, E. A., and R. W. Houghton (1998), Coastal ocean of equatorial west Africa from 10°N to 10°S, in *The Sea*, edited by A. R. Robinson and K. H. Brink, pp. 605–631, John Wiley & Sons.

Andrié, C., C. Oudot, C. Genthon, and L. Merlivat (1986), CO_2 fluxes in the tropical Atlantic during FOCAL cruises, *J. Geophys. Res.*, *91*(C10), 11,741–11,755.

Bakker, D. C. E., J. Etcheto, J. Boutin, and L. Merlivat (2001), Variability of surface water fCO_2 during seasonal upwelling in the equatorial Atlantic Ocean as observed by a drifting buoy, *J. Geophys. Res.*, *106*(C5), 9241–9253.

Bates, N. (2001), Interannual variability of oceanic CO_2 and biogeochemical properties in the Western North Atlantic subtropical gyre, *Deep Sea Res. II*, *48*, 1507–1528.

Bates, N., T. Takahashi, D. Chipman, and A. H. Knap (1998), Variability of pCO_2 on diel to seasonal timescales in the Sargasso Sea near Bermuda, *J. Geophys. Res.*, *103*(C8), 15,567–15,585.

Bates, N. R., L. Merlivat, L. Beaumont, and A. C. Pequignet (2000), Intercomparison of shipboard and moored CARIOCA buoy seawater fCO_2 measurements in the Sargasso Sea, *Mar. Chem.*, *72*(2–4), 239–255.

Chavez, F. P., P. G. Strutton, G. E. Friederich, R. A. Feely, G. C. Feldman, D. C. Foley, and M. J. McPhaden (1999), Biological and chemical response of the equatorial Pacific Ocean to 1997–98 El Niño, *Science*, *286*(5447), 2126–2131.

Copin-Montegut, C., M. Bégovic, and L. Merlivat (2004), Variability of the partial pressure of CO_2 on diel to annual time scales in the Northwestern Mediterranean Sea, *Mar. Chem.*, *85*, 169–189.

DeGrandpre, M. D., T. R. Hammar, S. P. Smith, and F. L. Sayles (1995), In situ measurements of seawater pCO_2, *Limnology and Oceanography*, *40*, 969–975.

Denman, K. L., and A. E. Gargett (1983), Time and space scales of vertical mixing and advection of phytoplankton in the upper ocean, *Limnology and Oceanography*, *28*(5), 801–815.

Dickson, A. G., and F. J. Millero (1987), A comparison of the equilibrium constants for the dissociation of carbonic acid in seawater media, *Deep Sea Res.*, *34*, 1733–1743.

González Dávila, M., J. M. Santana Casiano, M. J. Rueda, O. Llinás, and E.-F. González-Dávila (2003), Seasonal and interannual variability of sea-surface carbon dioxide species at the European Station for Times Series in the Ocean at the Canary Islands (ESTOC) between 1996 and 2000, *Global Biogeochem. Cycles*, *17*(3), 1076, doi:10.1029/2002GB001993.

Gouriou, Y., and G. Reverdin (1992), Isopycnal and diapycnal circulation of the upper equatorial Atlantic ocean in 1983–1984, *J. Geophys. Res.*, *97*(C3), 3543–3572.

Goyet, C., and E. T. Peltzer (1997), Variation of CO_2 partial pressure in surface seawater in the equatorial Pacific Ocean, *Deep Sea Research*, *44*(9/10), 1611–1626.

Hardman-Mountford, N. J., and J. M. McGlade (2003), Seasonal and interannual variability of oceanographic processes in the Gulf of Guinea: An investigation using AVHRR sea surface temperature data, *International Journal of Remote Sensing*, *24*(16), 3247–3268.

Herbland, A., and B. Voituriez (1979), Hydrological structure analysis for estimating the primary production in the tropical Atlantic Ocean, *Journal of Marine Research*, *37*, 87–101.

Hisard, P. (1980), Observation de réponses de type El Niño dans l'Atlantique tropical oriental Golfe de Guinée, *Oceanologica Acta*, *3*, 69–78.

Hood, E. M., and L. Merlivat (2001), Annual to interannual variations of fCO_2 in the northwestern Mediterranean Sea: Results from hourly measurements made by CARIOCA buoys, 1995–1997, *Journal of Marine Research*, *59*(1), 113–131.

Hood, E. M., L. Merlivat, and T. Johannessen (1999), Variations of fCO_2 and air-sea flux of CO_2 in the Greenland Sea gyre using high-frequency time series data from CARIOCA drift buoys, *J. Geophys. Res.*, *104*(C9), 20,571–20,584.

Hood, E. M., R. Wanninkhof, and L. Merlivat (2001), Short timescale variations of fCO_2 in a North Atlantic warm-core eddy: Results from the Gas-Ex 98 carbon interface ocean atmosphere (CARIOCA) buoy data, *J. Geophys. Res.*, *106*(2; Sect 3), 2561–2572.

Johnson, K. S., R. M. Pykowicz, and C. S. Wong (1979), Biological production and the exchange of oxygen and carbon dioxide across the sea surface in Stuart Channel, British Columbia, *Limnology and Oceanography*, *24*(3), 474–482.

Körtzinger, A., J. I. Hedges, and P. D. Quay (2001), Redfield ratios revisited: Removing the biasing effect of anthropogenic CO_2, *Limnology and Oceanography*, *46*(4), 964–970.

Kuss, J., W. Roeder, K.-P. Wlost, and M. D. DeGrandpre (2006), Time-series of surface water CO_2 and oxygen measurements on a platform in the central Arkona Sea (Baltic Sea): Seasonality of uptake and release, *Mar. Chem.*, *101*, 220–232.

Lee, K., L. T. Tong, F. J. Millero, C. Sabine, A. G. Dickson, A. G. Goyet, G.-H. Park, R. Wanninkhof, R. A. Feely, and R. M. Key (2006), Global relationships of total alkalinity with salinity and temperature in surface waters of the world's oceans, *Geophys. Res. Lett.*, *33*, L19605, doi:10.1029/2006GL027207.

Mehrbach, C., C. H. Culberson, J. E. Hawley, and R. M. Pytkowicz (1973), Measurement of the apparent dissociation constants of carbonic acid in seawater at atmospheric pressure, *Limnology and Oceanography*, *18*, 897–907.

Merle, J. (1980), Variabilité thermique annuelle et interannuelle de l'océan Atlantique équatorial Est. L'hypothèse d'un "El Niño" Atlantique, *Oceanologica Acta*, *3*(2), 209–220.

Molinari, R. L. (1982), Observations of eastward currents in the tropical South Atlantic Ocean: 1978–1980, *J. Geophys. Res.*, *87*(C12), 9707–9714.

Oudot, C. (1989), O_2 and CO_2 balances approach for estimating biological production in the mixed layer of the tropical Atlantic Ocean (Guinea Dome area), *Journal of Marine Research*, *47*, 385–409.

Oudot, C., C. Andrié, and Y. Montel (1987), Evolution du CO_2 océanique et atmosphérique sur la période 1982–1984 dans l'Atlantique tropical, *Deep Sea Research*, *34*(7), 1107–1137.

Oudot, C., J. F. Ternon, and J. Lecomte (1995), Measurements of atmospheric and oceanic CO_2 in the tropical Atlantic: 10 years after the 1982–1984 FOCAL cruises, *Tellus*, *47B*, 70–85.

Pérez, V., et al. (2005), Latitudinal distribution of microbial plankton abundance, production, and respiration in the Equatorial Atlantic in autumn 2000, *Deep-Sea Research I*, *52*, 861–880.

Piton, B., and A. Kartavtseff (1986), Utilisation de bouées dérivantes à positionnement par satellite pour une meilleure connaissance de l'hydrologie de surface du golfe de Guinée., *Doc. Sci. Cent. ORSTOM de Brest*, *34*, 1–41.

Rios, A., F. F. Pérez, M. Álvarez, L. Mintrop, M. González-Dávila, J. M. Santana Casiano, N. Lefèvre, and A. J. Watson (2005), Seasonal sea-surface carbon dioxide in the Azores area, *Mar. Chem.*, *96*, 35–51.

Servain, J., A. J. Busalacchi, M. J. McPhaden, A. D. Moura, G. Reverdin, M. Vianna, and S. E. Zebiak (1998), A Pilot Research Moored Array In the Tropical Atlantic (PIRATA), *Bulletin- American Meteorological Society*, *79*(10), 2019–2032.

Seyler, P., A. Coynel, P. Moreira-Turcq, H. Etcheber, C. Colas, D. Orange, J. P. Bricquet, A. Laraque, J. L. Guyot, and M. Meybeck (2003), *Organic carbon transported by the equatorial rivers: example of Zaire-Congo and Amazon Rivers*, Advances in Soil Science Editions, Ohio.

Smethie, W. M., T. Takahashi, D. W. Chipman, and J. R. Ledwell (1985), Gas exchange and CO_2 flux in the tropical Atlantic Ocean determined from ^{222}Rn and pCO_2 measurements, *J. Geophys. Res.*, *90*, 7005–7022.

Stramma, L., and F. Schott (1999), The mean flow field of the tropical Atlantic Ocean, *Deep Sea Res., II*, *46*, 279–303.

Wanninkhof, R. H. (1992), Relationship between wind speed and gas exchange over the ocean, *J. Geophys. Res.*, *97*(C5), 7373–7382.

Weiss, R. F. (1974), CO_2 in water and seawater: The solubility of a non-ideal gas, *Mar. Chem.*, *2*, 203–215.

Winn, C. D., Y. H. Li, F. T. Mackenzie, and D. M. Karl (1998), Rising surface ocean dissolved inorganic carbon at the Hawaii Ocean time-series site, *Mar. Chem.*, *60*(1–2), 33–47.

L. Beaumont and T. Danguy, DT INSU, 1 place Aristide Briand, 92195 Meudon, France.

A. Guillot, DT INSU, Bâtiment Institut Polaire, BP 74, 29280 Plouzané, France.

N. Lefèvre, IRD LOCEAN, Université Pierre et Marie Curie, 4 place Jussieu, 75252 Paris Cedex 05, France. (nathalie.lefevre@locean-ipsl.upmc.fr)